The estimation of detectability of GRB optical **orphan** afterglows with Gaia

J. Japelj and A. Gomboc

jure.japelj@fmf.uni-lj.si, andreja.gomboc@fmf.uni-lj.si

Faculty of Mathematics and Physics, University of Ljubljana, Slovenia

We expand our analysis of possible gamma-ray burst (GRB) optical afterglow detections with the Gaia satellite by including in our simulation also orphan afterglows. We explain theoretical background of the phenomenon and introduce parameters necessary in the simulation. We briefly describe the simulation process and conclude with the presentation and discussion of the results.

1 Orphan afterglows

GRB explosions are believed to be collimated, rather than spherical [1]. An indirect argument that supports this is based on the high values of energy output in gamma-rays ($\sim M_{\odot}c^2$) when considering a spherically symmetrical explosion. That kind of values are hard to produce in a model with stellar progenitor. Precise observations of an afterglow lightcurve can lead us to a more direct evidence: a break in the lightcurve. That can be well explained by considering a jet with a half-opening angle θ_{j}, moving initially at a relativistic speed with a high Lorentz factor $\Gamma \sim 100 - 1000$. Because of the relativistic beaming effect, the radiation emmited from the jet is beamed in an half-opening angle $\theta_{\mathrm{b}} = \frac{1}{\Gamma}$ in the direction of motion. The expanding jet is surrounded with a medium that causes the jet to decelerate. This results in an increasing value of the angle θ_{b}. Shortly after the prompt GRB emission we can not distinguish between a spherical and collimated explosion due to strong beaming, since $\theta_{\mathrm{j}} > \theta_{\mathrm{b}}$. But after some time, θ_{b} becomes larger than the opening angle of the jet itself. At that point the radiation flux drops and we can see that as an achromatic break in a lightcurve.

The shape of the lightcurve depends on the relative position of the observer's line-of-sight and the axis of the jet cone. We can describe that with an angle θ_{obs} between both directions. It is very unlikely for an observer to be looking precisely at the direction of the jet axis. We talk about an on-axis GRB and a 'regular' optical afterglow when $\theta_{\mathrm{obs}} < \theta_{\mathrm{j}}$. What if the jet cone is directed such that $\theta_{\mathrm{obs}} > \theta_{\mathrm{j}}$? Because of the beaming effect, an observer probably can not observe the prompt gamma emission. But the deceleration of the jet will gradually expand the beaming angle and the observer might detect the afterglow. The observation of an afterglow that was not preceded by a prompt gamma emission is called an orphan afterglow (OA)[1]. Even though OAs have not been conclusively detected yet, they have been studied a great deal over the last 15 years ([1] and references therein).

[1]The OAs we are discussing here are not to be confused with optical afterglows, for which the observer for some reason does not see the prompt gamma emission, even though the jet cone is directed into the observer's line of sight.

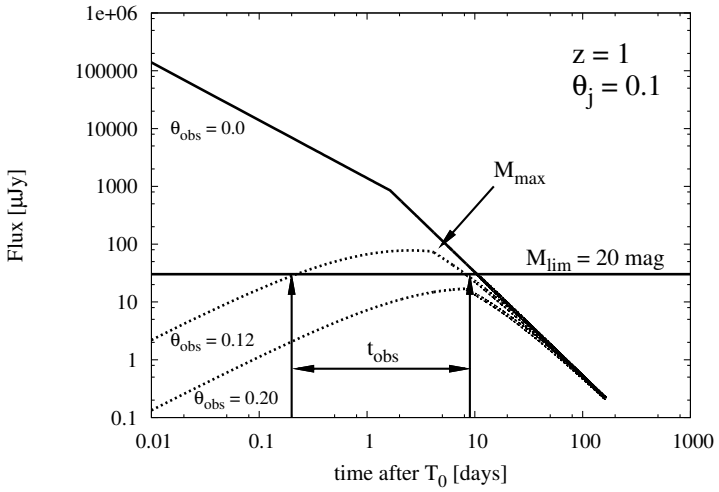

Figure 1: An example of an optical afterglow lightcurve ($\nu = 4.55 \times 10^{14}$ Hz) seen by an on-axis observer (full line) and the same event seen by an observer at an angle $\theta_{\rm obs} = 0.12$ and 0.20 (dotted lines). T_0 is the time at which the burst occured.

1.1 The lightcurve

There have been many semi-analytical models proposed to explain the dynamics of the jet and consequently the shape of the OAs lightcurve. In our simulation, we follow the approach of [2], which in itself is based on [3] and [4], where an adiabatic jet with a half-opening angle $\theta_{\rm j}$ and without sideways expansion is considered. The latter is a good approximation for a highly relativistic jet, as have been shown in hydrodynamical simulations [1].

With the knowledge of the jet half-opening angle $\theta_{\rm j}$, its total kinetic energy $E_{\rm j}$, redshift z and the density n of the circum-burst medium, we can compute the time $t_{\rm j}$, at which an on-axis observer will see the break in a lightcurve, and the flux density $F_{\nu,{\rm j}} = f(t_{\rm j}, E_{\rm j}, D_{\rm L}, z, \nu, p, \varepsilon_{\rm e}, \varepsilon_{\rm B})$ at that time (equations (2) and (3) in [2]); $D_{\rm L}$ stands for luminosity distance, p is the power-law index of shock-accelerated electrons and $\varepsilon_{\rm e}$ and $\varepsilon_{\rm B}$ are the energy equipartition factors of the electrons and magnetic field, respectively. The rest of the lightcurve is obtained by applying the power-law temporal decay with a pre-break temporal index $\alpha_1 = 1$ and a post-break index $\alpha_2 = \alpha_1 + 3/4$ [2].

The lightcurve seen by an off-axis observer is obtained by considering a point source approximation [4]:

$$F_\nu(\theta_{\rm obs}, t) = a^3 F_{\nu/{\rm a}}(0, at), \tag{1}$$

where $a \equiv (1-\beta)/(1-\beta\cos\theta_{\rm obs})$ and $\beta = \sqrt{1-1/\Gamma^2}$. This approach works only in the case of $\theta_{\rm obs} > \theta_{\rm j}$. The changing of the Lorentz factor is described with[4]:

$$\Gamma(t) = \begin{cases} \theta_{\rm j}^{-1} \left(\frac{t}{t_{\rm j}}\right)^{-3/8} & t < t_{\rm j} \\ \theta_{\rm j}^{-1} \left(\frac{t}{t_{\rm j}}\right)^{-1/2} & t > t_{\rm j} \end{cases} \tag{2}$$

In Figure 1 three afterglow lightcurves are shown for the case of $\theta_{\rm j} = 0.1$ and $z = 1$. The flux is calculated for a frequency of $\nu = 4.55 \times 10^{14}$ Hz. The full lightcurve corresponds to an on-axis observer, while the dotted ones represent the lightcurves seen at angles $\theta_{\rm obs} = 0.12$ and 0.20, i.e. lightcurves of OAs. The lightcurves of OAs cannot be observed shortly after the prompt burst. But the flux slowly rises and eventually reaches the peak value, after which it begins to decay again. Depending on the parameters mentioned in this section, the OA's lightcurve can be seen during the period in which OA's flux is above the observer's detection limit (corresponding to the observer's limiting magnitude $M_{\rm lim}$).

In our simulation, the following parameter values have been used: $E_{\rm j} = 1 \times 10^{51}$ erg, $p = 2.2$, $\varepsilon_{\rm e} = 0.1$, $\varepsilon_{\rm B} = 0.01$, $\nu = 4.55 \times 10^{14}$ Hz. Other parameters are discussed in the next section.

2 Simulation parameters

The simulation is done in much the same way as in the case of our first analysis [5]. Again, we generate a number of events, distributed randomly (but uniformly) in the sky and randomly (but uniformly) in time. Since the OAs have not been observed yet, we do not have any data available to base the number of observable OAs on. In addition, we can not simply generate an initial distribution of OA's magnitudes. We approach the problem by constructing a number of OA's lightcurves with characteristics from theoretical predictions. For a given lightcurve, it is then verified whether it rises above the limiting flux or not. In the former case, the time interval $t_{\rm obs}$ in which the OA can be observed is calculated. If during this time interval the position of the burst comes into the field of view of one of the Gaia's telescopes, we consider that the afterglow was detected.

We already explained the procedure of constructing the lightcurve in section (1.1), where we assigned typical values to some of the parameters needed in the calculation of the lightcurve. In the simulation, we assign the same value of $E_{\rm j}$ to all generated bursts, since it is believed that otherwise differing observed energy values correspond to different jet half-opening angle values [2] and we don't expect that this will have substantial effect on our results. Other parameters needed in the simulation are explained in this section.

2.1 Number of GRBs

Several estimations of the detectability of OAs have been made [2][6]. Because the obtained results depend on the jet models, initial half-opening angle distribution, the medium surrounding the GRB source etc., we decided to take a simple estimation of the number of all GRBs that occur in the universe up to some redshift z. During the simulation, the events with $\theta_{\rm obs} < \theta_{\rm j}$ are then sorted out and we are left only with the bursts for which the OA lightcurves can be generated.

Following [7] the GRB formation rate is taken as

$$R_{\rm GRB} = R_{\rm SFR} = \rho_0 \begin{cases} 10^{0.75z} & z < 1 \\ 10^{0.75} & z \geq 1, \end{cases} \tag{3}$$

where $R_{\rm SFR}$ represents the Rowan-Robinson star formation rate [8] and $\rho_0 \sim 33\ h_{65}^3$ Gpc^{-3} yr^{-1} [7]. Considering the expansion of the universe (which is taken to be flat, i.e. $\Omega_k = 0$), the number of bursts dN that occure between redshift z and $z + dz$ in one year is:

$$dN(z) = \frac{R_{\rm GRB}}{1+z} \frac{dV}{dz} dz, \tag{4}$$

where the division factor $(1 + z)$ is due to the time dilation and the comoving volume element dV/dz equals

$$\frac{dV}{dz} = \frac{c}{H_0} \frac{4\pi\chi^2(z)}{E(\Omega_{\rm i}, z)}, \qquad \chi(z) = \frac{c}{H_0} \int_0^z \frac{dz'}{E(\Omega_{\rm i}, z')} \tag{5}$$

with $E(\Omega_{\rm i}, z) = \sqrt{\Omega_{\rm m}(1+z)^3 + \Omega_\Lambda}$. The number of GRBs per year equals

$$N = \int_0^{z_{\rm max}} \frac{R_{\rm GRB}}{1+z} \frac{dV}{dz} dz. \tag{6}$$

In our calculation, we adopt standard cosmology of a flat universe with $h = 0.72$, $\Omega_m = 0.3$ and $\Omega_\Lambda = 0.7$ and set $z_{\rm max} = 5$. Thus calculated number of GRBs that occure per year is $N \sim 25000$.

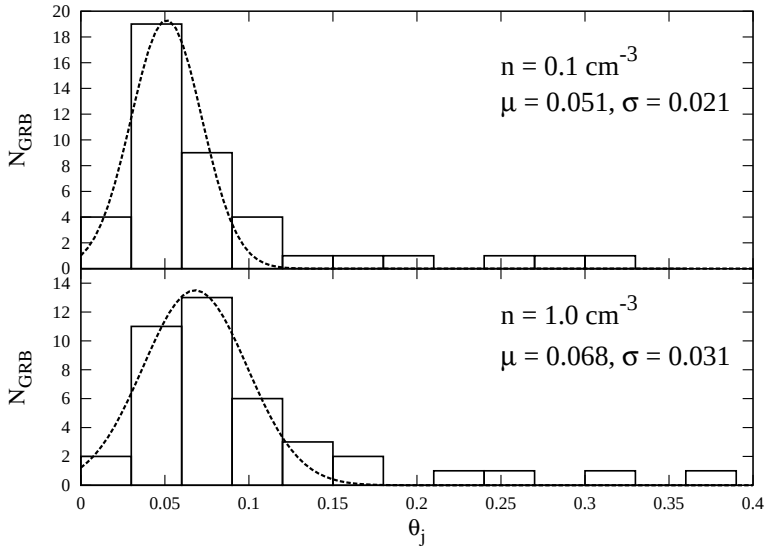

Figure 2: The distribution of calculated jet half-opening angles $\theta_{\rm j}$ for two different values of n. In each case, the distribution is fitted with a normal distribution with the mean value μ and standard deviation σ.

2.2 GRB redshift distribution

In our simulation we generate the redshift distribution of GRB events according to equation (4) in the following way. The probability of finding a GRB at redshift z is [9]:

$$p(z) = \frac{(dN/dz)}{\int_0^{z_{\rm max}}(dN/dz)dz}. \tag{7}$$

Next, a cumulative function $P(z)$ can be calculated:

$$P(z) = \int_0^z p(z^{'})dz^{'}, \tag{8}$$

giving the probability of an event occuring in the redshift range 0 to z. By calculating the inverse of $P(z)$, the redshift as a function of the cumulative probability is obtained. Employing a random number generator to select values $P(z)$, a GRB redshift distribution according to equation (4) is obtained.

2.3 Jet half-opening angle distribution

Not many GRB afterglows have been observed with a high enough precision to enable us the determination of $\theta_{\rm j}$, which can be calculated as [10]

$$\theta_{\rm j} = 0.057 \left(\frac{t_{\rm j}}{1\ {\rm day}}\right)^{3/8} \left(\frac{1+z}{2}\right)^{-3/8} \left(\frac{E_{\rm iso}(\gamma)}{10^{53}\ {\rm erg}}\right)^{-1/8} \left(\frac{n_\gamma}{0.2}\right)^{1/8} \left(\frac{n}{0.1\ {\rm cm}^{-3}}\right)^{1/8}, \tag{9}$$

where $E_{\rm iso}(\gamma)$ is the gamma energy output in the case of a spherical burst, n_γ the efficiency in converting the energy of the ejecta into gamma-rays and n the number density of the circum-burst medium.

Using (9), we calculated angles $\theta_{\rm j}$ for 43 GRBs from observational data collected in Table 1 in [11]. The angle distribution is shown in Figure 2. In our calculation, we set $n_\gamma = 0.2$. We present the results for two different values of number density. The distributions have been fitted with a normal distribution function. In the simulation, random generated half-opening angles are taken to be distributed according to these two functions. The simulation is ran for each number density case separately. As an additional constraint we generate only angles greater than $\theta_{\rm j} = 0.01$ rad.

An important parameter in the simulation is the observational angle $\theta_{\rm obs}$, which is distributed uniformly between 0 and π (because of jet bimodality).

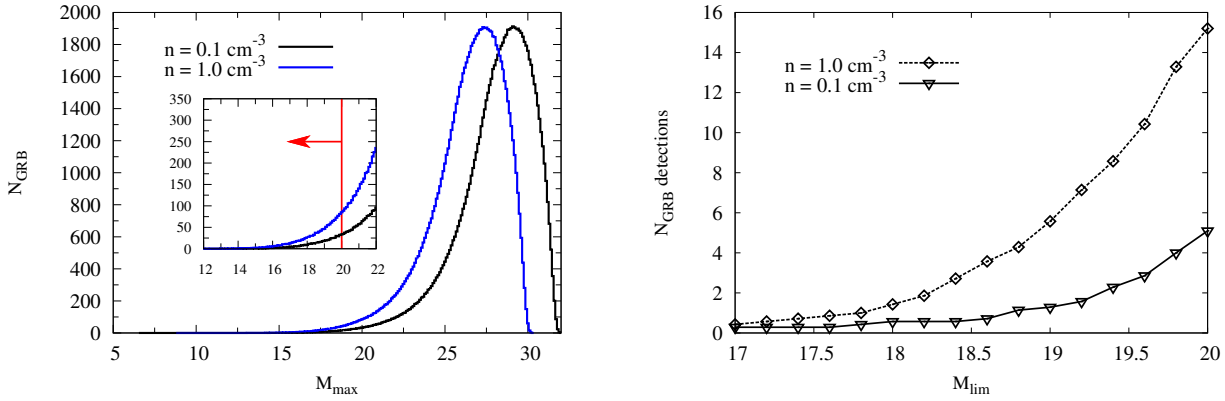

(a) (b)

Figure 3: (a) The distribution of peak OA's lightcurve values $M_{\rm max}$ for two different values of surrounding medium number density n. The lower part of the distribution is zoomed in a separate window, where the red arrow marks the events that can be detected in the case of $M_{\rm lim} = 20$ mag. (b) GRB OAs detection rate in five years of Gaia's operation as a function of $M_{\rm lim}$.

3 Results and discussion

Here we present the results of the simulation. All results are given for a time period of five years, which is the expected operational time of Gaia. All the results are averaged over 100 simulations unless stated otherwise. In Figure 3*a* we show the distribution of the lightcurve peak values $M_{\rm max}$ (Figure 1) for two different values of n. It has already been explained in section 2.1 how, out of all generated GRBs, we consider only those that have $\theta_{\rm obs} > \theta_{\rm j}$, i.e. those that actually represent OAs. The bursts that satisfy $\theta_{\rm obs} > \theta_{\rm j}$ are plotted in Figure 3*a*. The two distributions are similar. The lower part of Figure 3*a* is zoomed and shown in a separate window, where the red arrow indicates which OAs could be detected in the case of $M_{\rm lim} = 20$ mag, which is the expected limiting magnitude for Gaia. The number of OAs with higher peak flux is greater in a case of high density environment. That is because $F_{\rm j}$ is actually proportional to $n^{(3-p)/12}$ (equation (3) in [2]).

The number of detected OAs as a function of $M_{\rm lim}$ is shown in Figure 3*b*. The greater detection number in the case of high density environment agrees with already discussed fact, that OAs are brighter if n is larger. Also, the larger distribution difference in Figure 3*a* results in a larger detection difference. The expected number of OA detections in the case of $M_{\rm max} = 20$ is ~ 15.

In Figure 4*a* we show the correlation between redshift z and jet half-opening angle $\theta_{\rm j}$. The data shown here were obtained over 100 simulations and correspond to the OAs detected with one of Gaia's telescopes (black points) and both telescopes (red points) in the case of $M_{\rm lim} = 20$ mag. As expected, most $\theta_{\rm j}$ values are concentrated around the peak of $\theta_{\rm j}$ distribution (section 2.3). Most points have values of $z < 2$. That can be understood, since high redshift value results in a lesser observed flux. Also, the GRB redshift distribution (section 2.2) has a peak at $z = 1$ after which the number of GRBs starts to decline. However, a few OAs with high redshift are detected in the simulation. Since all of those OAs have relatively low $\theta_{\rm j}$, which neutralize the negative redshift effect on the flux values, their detection is understandable. Majority of second detections have low redshift values and no preferable $\theta_{\rm j}$. However, that is mostly because of the distribution of first detections. Because of the relatively flat lightcurve around the peak value (Figure 1), once the OA has been detected with the first telescope, redshift and $\theta_{\rm j}$ are not the most important parameters for the second detection. In order to detect OA with the second telescope, the time at which it is first detected, i.e. before or after the peak flux value, is important.

In Figure 4*b* the correlation between redshift z and observing angle is shown. One has to bear in mind, that the observing angle has to be greater than the half-opening angle for a particular burst.

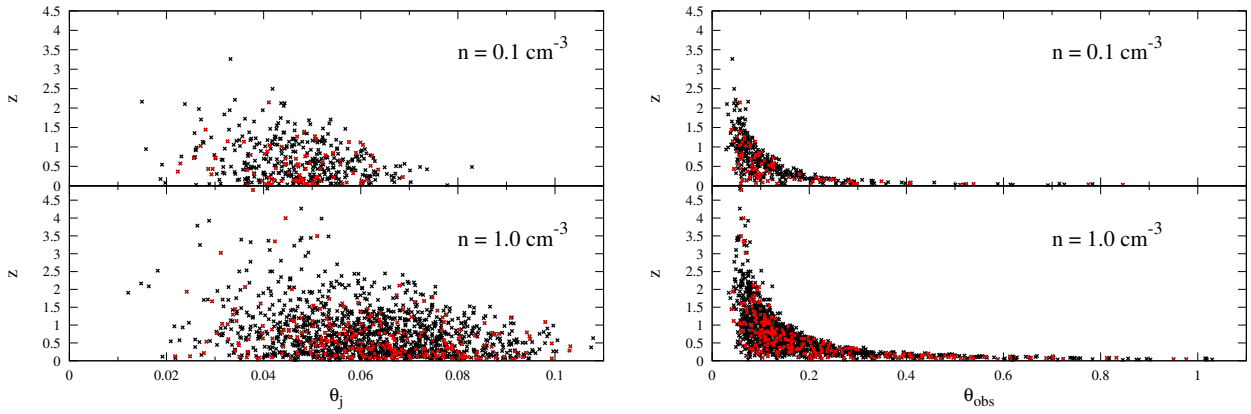

Figure 4: Correlation between redshift z and (a) jet half-opening angle $\theta_{\rm j}$ and (b) observing angle $\theta_{\rm obs}$ for detected OAs in the case of $M_{\rm lim} = 20$ mag. The data shown were obtained over 100 simulations and correspond to the OAs detected with one telescope (black points) and both telescopes (red points).

If a burst has a low redshift, an observing angle can be quite large, as is shown in the long tail. On the other hand, very low observing angle can result in the detection of an OA from a distant object, since the difference between $\theta_{\rm j}$ and $\theta_{\rm obs}$ is not very large. Detections with the second telescope do not appear to have a preferable position in the graph.

The results are clearly dependant on a set of various parameters, as is evident from the analysis above. A more detailed analysis has only been made to understand the dependance of the results on the different density of the GRB environment. However, we made other assumptions and simplifications in the course of simulation preparation, which are described in sections 1.1 and 2. Thus the results have to be interpreted with all these reservations in mind.

Now we can compare the results of this simulation with the previous one, where only on-axis afterglows have been considered [5]. Only the results obtained in the case of $M_{\rm lim} = 20$ mag are discussed here. In [5] we showed that the expected number of detected on-axis afterglows in five

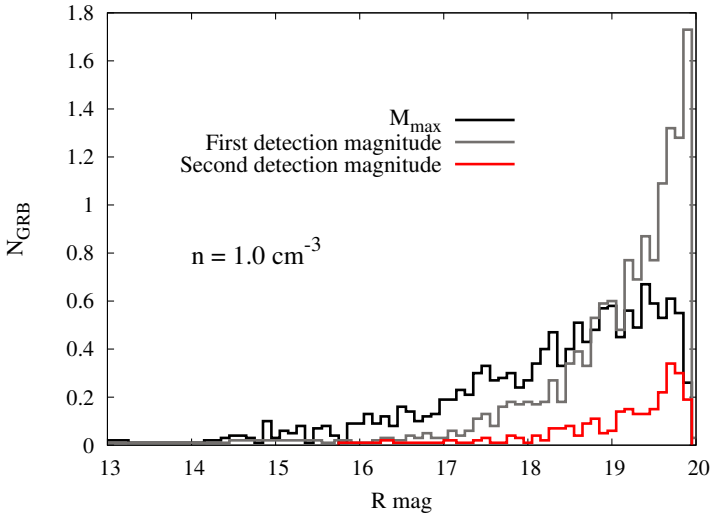

Figure 5: Distribution of magnitudes $M_{\rm max}$, associated with detected afterglows (black), magnitudes at the time of the first detection (grey) and magnitudes of afterglows detected also by the second telescope (red). The results are given for a five year simulation.

years is almost negligible. This simulation shows that the afterglow detection rate could improve with the addition of OAs, though not very much. In Figure 5 magnitude distribution of detected OAs is shown. This figure is similar to Figure 3*b* in [5]. The distribution of magnitudes in the case of $n = 0.1$ cm^{-3} is not given here, since it strongly resembles that of $n = 1.0$ cm^{-3} (but the number of simulation detections is lower). The fraction of detections with the second telescope is similar in both simulations. In [5], the power-law temporal decay index was taken to be $\alpha = 0.7$, while in OA simulation we assume $\alpha = 1.0$. Even though α is not equal in those two groups of simulations, the comparison is still valid, i.e. more OAs could be detected than on-axis afterglows. We ran OAs simulation for the case of $n = 1.0$ cm^{-3} with a pre-break index $\alpha = 0.7$. Since the decay is not as steep, the detection rate is somewhat larger, i.e. ~ 35 detections in five years (compared to ~ 15 for $\alpha = 1.0$).

Even though the number of possible afterglow detections increased with the inclusion of OAs in our simulations, the change in magnitude throughout the observation with one telescope will be two small to detect it (details in [5]). Still, the possibility for afterglow recognition might be possible with the characteristical color indices [5].

4 Conclusions

We have shown in this simulation that the number of expected OA detections with the Gaia satellite during it's five years of expected operation is of the order of 10. Adding the results of the on-axis afterglows simulation [5], the number of expected optical afterglow detections in five years is slightly increased. The problem of afterglow recognition and poor time sampling of the lightcurve, in addition to the small number of expected detections, makes the study of GRB optical afterglows with Gaia difficult. On the other hand, since OAs have not been detected yet, a possible detection would provide valuable new data.

References

[1] J. Granot, 2006, arXiv:astro-ph/0610379v1

[2] Y. C. Zou, X. F. Wu & Z. G. Dai, 2006, arxiv:astro-ph/0601292v2

[3] X. F. Wu, Z. G. Dai & E. W. Liang, 2004, Apj, 615, 359

[4] J. Granot, A. Panaitescu, P. Kumar, S. Woosley, 2002, arXiv:astro-ph/0201322v2

[5] J. Japelj, A. Gomboc, The estimation of detectability of on-axis GRB optical afterglows with Gaia ($http://www.ast.cam.ac.uk/research/gsawg/index.php/Triggers:GRBs$)

[6] T. Totani, A. Panaitescu, 2002, Apj, 576, 120

[7] D. Guetta, T. Piran, E. Waxman, 2004, arxiv:astro-ph/0311488v5

[8] M. Rowan-Robinson, 1999, Ap&SS, 266, 291

[9] D. M. Coward, R. R. Burman, D. G. Blair, 2002, MNRAS, 329, 411

[10] D. A. Frail et al., 2001, arXiv:astro-ph/0102282v1

[11] Y. Gao, Z. G. Dai, 2009, arXiv:astro-ph/0911.1579v1